TELKOMNIKA Telecommunication, Computing, Electronics and Control
Vol. 19, No. 3, June 2021, pp. 950~956
ISSN: 1693-6930, accredited First Grade by Kemenristekdikti, Decree No: 21/E/KPT/2018
DOI: 10.12928/TELKOMNIKA.v19i3.15832

The impacts of red-emitting phosphor $Mg_8Ge_2O_{11}F_2:Mn^{4+}$ on the color rendering index of convex-dual-layer remote phosphor WLEDs at 5600 K

My Hanh Nguyen Thi[1], Phung Ton That[2], Nguyen Doan Quoc Anh[3]
[1]Faculty of Mechanical Engineering, Industrial University of Ho Chi Minh City, Vietnam
[2]Faculty of Electronics Technology, Industrial University of Ho Chi Minh City, Vietnam
[3]Power System Optimization Research Group, Faculty of Electrical and Electronics Engineering, Ton Duc Thang University, Ho Chi Minh City, Vietnam

Article Info

Article history:

Received Feb 14, 2020
Revised Nov 17, 2020
Accepted Dec 7, 2020

Keywords:

Luminous flux
$Mg_8Ge_2O_{11}F_2:Mn^{4+}$
Mie-scattering theory
WLEDs

ABSTRACT

The poor color rendering index (CRI) induced by mono chip and phosphor configuration in the conventional white-light light-emitting diode (LED) urges for developments in both packaging and material, thus, a modern lighting solution was introduced. The dual-layer phosphor package is an innovative configuration that can retain the lumen output of conventional white light emitting diode (WLED) while also enhancing color quality. The structure of dual-layer phosphor package that was proposed includes two chips and one phosphor. The priority in this research is to keep improving the lighting properties of WLED, therefore, further experiments with this dual-chips and dual-phosphor package are conducted. The lighting properties of LED are measured multiple times with its nitride-based phosphor being altered in proportions and densities each occasion, the results are calculated with a color design model made specifically to monitor and adjust the color of white-light from LED to match desired outcome. The WLED at 5600 K correlated color temperature (CCT) is the sole research object of the experiments. The measured parameters from the 5600 K WLED and the color coordinates of CIE 1931 simulated from the color design model show that 0.0063 is the highest possible discrepancy at 5600 K (CCT). The information from this manuscript provide the manufacturers with the most efficient approach to create a white LED that has good color quality, high CRI and luminous flux.

Corresponding Author:

Nguyen Doan Quoc Anh
Power System Optimization Research Group, Faculty of Electrical and Electronics Engineering
Ton Duc Thang University
No. 19 Nguyen Huu Tho Street, Tan PhongWard, District 7, Ho Chi Minh City, Vietnam
Email: nguyendoanquocanh@tdtu.edu.vn

1. INTRODUCTION

Lighting devices that emit white light by converting phosphor materials (pc-LEDs) is an outstanding lighting solution with formidable performance in terms of life expectancy, manufacturing cost, lighting efficiency, endurance against impacts, and space-saving, thus, received growing attention in the lighting industry [1-3]. The white LED is expected to replace conventional lighting methods, although as the lighting demands evolve, the white light emitting diode (WLED) need to enhance their advantages while improving

the existing weakness [4-6]. The evidence is that with the recognition that WLED has acquired, it is being utilized in not only indoor but also in harsh conditions of outdoor lighting, and recent discovery in fast-witch, WLED is now an essential part of smart lighting and other automatic technologies [7-9]. To keep pressing the growing pace, WLED must achieve further improvements, especially in color rendering index (CRI), an aspect that WLED usually struggle with [10-12]. The color rendering index (CRI), which is the result from the comparison between LED light and natural sunlight or black-body radiation, is the most commonly used parameter to evaluate the quality of light from an LED. The light source with wider spectrum is closer to the ideal emission range of black-body radiation and has better rendering ability, which reflects in the color quality [13, 14]. There are several method that have been proposed to constitute white light, yet combining one blue chip and one yellow phosphor in an LED package is the most commonly for the cheap cost and convenient for mass production. However, the problem with this method is the low emission spectra so that the WLED created this way cannot fully exploit the light at higher wavelength resulting in poor CRI and low light quality. The solution of adding one more chip alongside the blue one and the yellow phosphor was proposed for this issues that there are many results from previous reports have confirmed the effectiveness of the additional phosphors in enhancing LEDs emission spectrum leading to high color quality color and CRI [15-18].

The LED parameters along with the emission spectrum of phosphor are measured and extensively studied using empirical and mathematical models, and the results provide useful knowledge in the development of light color and CRI. However, a systematic method to create a pc-LEDs with tunable color temperature, good lumen output, and chromatic performance is yet to be found. Solutions were proposed to achieve this goal and two methods were able to yield notable results despite still having drawback. The first one is using a dual-phosphor LED to obtain high CRI, however, the lighting efficacy from this solution is not very remarkable due to Stokes Shifts. The second solution applies an dual-chip configuration with individual red and blue chips with conventional phosphor material that exhibits excellent results in color quality and light output although the color unchangeable. Therefore, combining these two solutions and using a LED package with two chips and two phosphors is the suggested idea to obtain all three requirements of high CRI, luminous efficacy and tunable color. Using Beer's law [19-22] and linear conversion in the lighting device simulation process, we introduce a color design model that can slightly adjust the chromatic indication. The simulated WLED model consists of the yellow-emitting YAG:Ce phosphor and high performance chromatic LED chips. Being a material that is fairly easy to create, the $MgSr_3Si_2O_8:Eu^{2+}$ phosphor minimizes the cost on the manufacturing process and not to mention the great and consistent lighting performance at high temperature which rendered $MgSr_3Si_2O_8:Eu^{2+}$ phosphor as an excellent material for the construction of heavy duty and high durability lighting devices. The nitride-based phosphor we have chosen to include in the experiments is the $MgSr_3Si_2O_8:Eu^{2+}$ phosphor that emits deep red light at 681 nm wavelength. The white LEDs used in the experiments have different phosphor proportions and densities and two types of red LEDs to ensure the accuracy as well as diversity of the research result. The suitability and simplicity in application of the color design model are proven through the research process.

2. EXPERIMENT

2.1. Preparation

The red phosphor used in the experiments is $Mg_8Ge_2O_{11}F_2:Mn^{4+}$, a type of phosphor that has a deep red light emission and reach 1.88 eV emission power at peak. The red-light component added from $Mg_8Ge_2O_{11}F_2:Mn^{4+}$ will strengthen the chromatic quality and allow the color of white light to be adjusted. The process of making $Mg_8Ge_2O_{11}F_2:Mn^{4+}$ consists of 3 main steps: mixing, firing and re-firing. First, mix the ingredients for $Mg_8Ge_2O_{11}F_2:Mn^{4+}$ by ball-milling. After that, place the compound in capped quartz tubes filled and burned at 1200°C for 2 hours. The product from the first firing process is a solid lump that to be ball-milling in to powder before starting the next firing process. In the second firing process, use open quartz tubes filled with air to contain the powder, then put it the furnace at 1200°C for about 16 hours (overnight). The producing process of $Mg_8Ge_2O_{11}F_2:Mn^{4+}$ need to be followed strictly to ensure the quality of the phosphor outcome, the final product from the process is store in a sealed container to avoid contamination.

2.2. Simulation

The LightTools program and Mie-theory are the primary tools to create the simulation of dual-layer phosphor WLEDs, see Figure 1 (a). The WLED simulation is applied to the measurement of phosphor scattering properties and the results from which are used to evaluate the influences of $Mg_8Ge_2O_{11}F_2:Mn^{4+}$ phosphor on the performance of the WLEDs at 5600 K CCT. The red phosphor $Mg_8Ge_2O_{11}F_2:Mn^{4+}$ and yellow phosphor $YAG:Ce^{3+}$ are combined and placed in the in-cup phosphor configuration as illustrated in Figure 1 (b) and Figure 1 (c). The phosphor layers of WLEDs are formed by merging the red phosphor,

yellow phosphor, and the silicone resin. Figure 1 (d) demonstrates the packaging order of WLED which show 9 blue chips at the bottom covered by reflector cups, phosphor layers and a silicone layer. The reflectors used in the simulator are 2.07x8x9.85 mm in height, base and summit are. Each chip contained in the reflector emits an 1.16 W at the highest lighting intensity of 453 nm, and the refractive index of red phosphor $Mg_8Ge_2O_{11}F_2:Mn^{4+}$ is 1.85 and yellow phosphor YAG:Ce^{3+} 1.83. The concentrations of $Mg_8Ge_2O_{11}F_2:Mn^{4+}$ and YAG:Ce^{3+} are constantly balance against each other to stabilize the ACCTs.

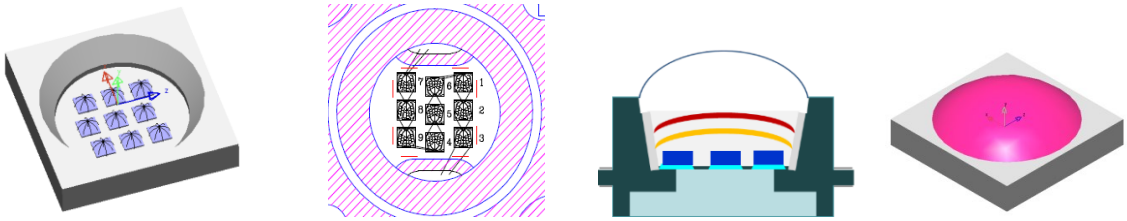

Figure 1. (a) 3D modelling, (b) Bonding diagram, (c) WLEDs packaging order, and (d) LightTools simulated WLEDs model

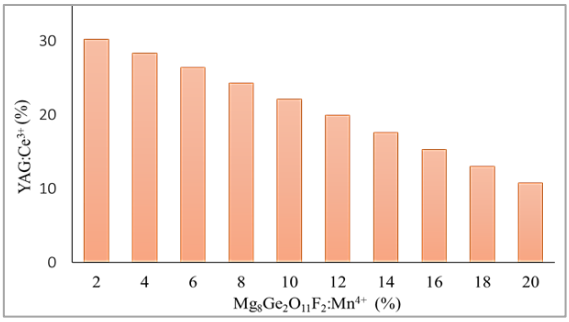

Figure 2. The balancing between $Mg_8Ge_2O_{11}F_2:Mn^{4+}$ and YAG:Ce^{3+} concentrations to maintain the average CCT

3. COMPUTATION AND DISCUSSION

Figure 2 illustrate the balancing of red phosphor $Mg_8Ge_2O_{11}F_2:Mn^{4+}$ and yellow phosphor YAG:Ce^{3+} to maintain the ACCT. The graph show that the concentration of $Mg_8Ge_2O_{11}F_2:Mn^{4+}$ and YAG:Ce^{3+} are disproportional, which means as the concentration of $Mg_8Ge_2O_{11}F_2:Mn^{4+}$ increases from 2-26% wt., the concentration of YAG:Ce^{3+} must be decreased accordingly. The adjustment of YAG:Ce^{3+} concentration in the opposite direction of $Mg_8Ge_2O_{11}F_2:Mn^{4+}$ can keep the average CCTs and can also modify the emission and absorption properties of phosphor layers that affect the WLEDs color quality and light output. These results prove the influence of $Mg_8Ge_2O_{11}F_2:Mn^{4+}$ on the performance of WLEDs at 5600 K color temperature.

The impact of red phosphor $Mg_8Ge_2O_{11}F_2:Mn^{4+}$ on the emission spectra of WLEDs are demonstrated in Figure 3. In 5600 K WLED, the white light is yielded from the special regions shown in this graph. The red line, which demonstrate the phosphor concentration at 20%, indicates a light emission increase in wavelength band from 648–738 nm, in comparison to the insignificant changes when the concentration is at 2%. The spectral development that $Mg_8Ge_2O_{11}F_2:Mn^{4+}$ bring to the phosphor in WLEDs is outstanding considering how the lighting intensity at 420-480 nm wavelength and 500-640 nm wavelength both rise with the presence of $Mg_8Ge_2O_{11}F_2:Mn^{4+}$ disregarding the amount. The spectral increases at 420-480 nm and 500-640 nm also known to excite the scattering properties of blue light. Another element that also affect the emission spectra of WLED is the color temperature, which boost the emission spectra as it gets higher. Thus, the $Mg_8Ge_2O_{11}F_2:Mn^{4+}$ phosphor is proven to not only effective in enhancing emission spectra of WLEDs with low color temperature such as 5600 K but also WLED with high color temperature up to 7700K. This is an important point in applying $Mg_8Ge_2O_{11}F_2:Mn^{4+}$ phosphor and managing the light quality of WLEDs. However, high color quality WLEDs may experience a small decrease in luminous flux. With that being said, the manufacturers have to choose the concentration level suitable for the production of WLEDs that satisfy their demands.

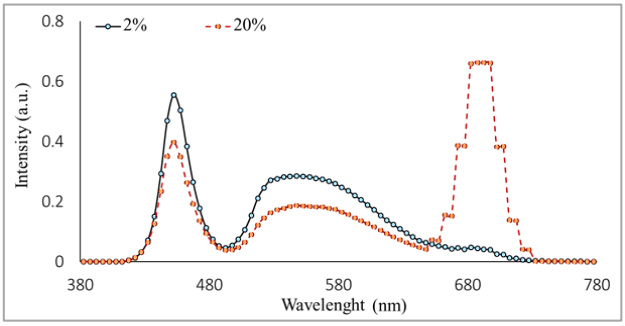

Figure 3. The emission spectra changes according to $Mg_8Ge_2O_{11}F_2:Mn^{4+}$ concentration in 5600 K WLEDs

Figure 4 illustrates how color rendering index (CRI) changes when there is $Mg_8Ge_2O_{11}F_2:Mn^{4+}$ phosphor in WLED package. As Figure 4 suggests, the CRI rise with $Mg_8Ge_2O_{11}F_2:Mn^{4+}$ concentration at all concentration levels from 2-20%, which is the result of the $Mg_8Ge_2O_{11}F_2:Mn^{4+}$ absorption properties. After absorbing the light from the blue chip, the phosphor particles from $Mg_8Ge_2O_{11}F_2:Mn^{4+}$ transform the blue light into red light. Although $Mg_8Ge_2O_{11}F_2:Mn^{4+}$ also absorb yellow light along with the blue light from LED chip, however, red light component is still dominant as $Mg_8Ge_2O_{11}F_2:Mn^{4+}$ absorb more blue light due to the nature of the material. Therefore, the color rendering index (CRI) is improved when the red phosphor $Mg_8Ge_2O_{11}F_2:Mn^{4+}$ is available because of the increased red-light component. High CRI in WLED means the chromatic performance is good and increase the market value of the WLED, however, it also means the manufacturing cost will be higher. This is when the cost effectiveness of $Mg_8Ge_2O_{11}F_2:Mn^{4+}$ become useful because it lowers the manufacturing cost of WLEDs and make red phosphor $Mg_8Ge_2O_{11}F_2:Mn^{4+}$ suitable for mass production.

CRI is the most common quality indicator, yet the assessment scope of CRI is fairly limited, so to say the quality of a WLED is good. Therefore, solely rely on the CRI to evaluate may not be sufficient. As a result, color quality scale (CQS) a quality indicator that includes the color rendering index, the preference of the viewer, and the color coordinates, is better for further assessment of WLEDs quality and more reliable. Figure 5 presented the calculated CQS in dual-phosphor WLED with $Mg_8Ge_2O_{11}F_2:Mn^{4+}$ phosphor. The CQS rises by a huge margin when red phosphor $Mg_8Ge_2O_{11}F_2:Mn^{4+}$ concentration increases. The enhanced CQS is significant and confirms the effectiveness of red phosphor $Mg_8Ge_2O_{11}F_2:Mn^{4+}$ in color quality development of dual-layer phosphor structure. This is an important finding regarding how impactful it is to the increase of color quality, however, applying red phosphor $Mg_8Ge_2O_{11}F_2:Mn^{4+}$ can damage the luminous flux which is presented in Figure 6. The mathematical model provided in the next part is the tools to study the cause behind this phenomenon. The calculation of blue radiation and yellow light conversion in the double-layer phosphor structure are presented. These are the two important features that can directly affect the performance of LEDs. The uneven lighting distribution of single LED configuration is usually computed by Gaussian function [23-26]:

$$P_\lambda = P_{opt}\frac{1}{\sigma\sqrt{2\pi}}exp\left[-0.5*\frac{(\lambda-\lambda_{peak})^2}{\sigma^2}\right] \quad (1)$$

In which, σ is dependent on highest wavelength λ_{peak}, while FWHM Δλ is yielded from the following (2).

$$\sigma = \frac{\lambda^2_{peak}\Delta E}{2hc\sqrt{2\,ln\,2}} = \frac{\lambda^2_{peak}\left(\frac{hc}{\lambda_1}-\frac{hc}{\lambda_2}\right)}{2hc\sqrt{2\,ln\,2}} = \frac{\lambda^2_{peak}\left(\frac{hc\Delta\lambda}{\lambda_1\lambda_2}\right)}{2hc\sqrt{2\,ln\,2}} \quad (2)$$

The lighting energy of lighting configuration utilizing yellow YAG phosphor and blue LED chip can hypothetically be considered as the common emission wavelength range between the two chromatic light spectra. Practically speaking, yellow phosphor emits energy in yellow spectrum and part of green light. Therefore, calculating the emitted energy of green emission spectrum and compares it to the conventional SPD with blue and yellow spectra can point out the changes that dual-layer configuration bring to light quality. In this manner, the green wavelength range is added to the dual-layer model and form triple spectrum model (B-G-Y), which results is represented in (3) and consequently replaced by (4).

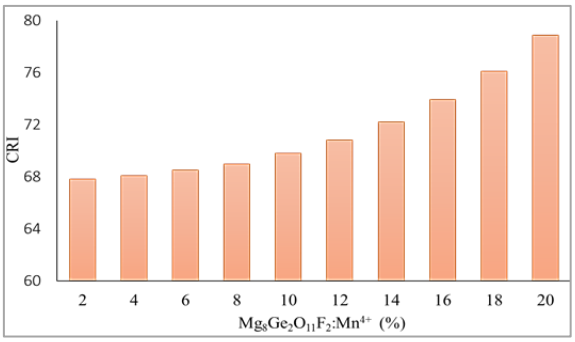

Figure 4. The correspondence between the color rendering index and $Mg_8Ge_2O_{11}F_2:Mn^{4+}$ concentration in 5600 K WLEDs

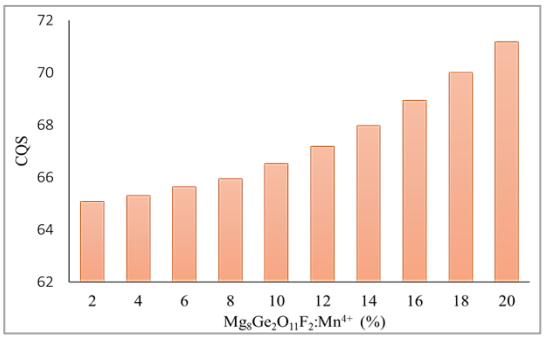

Figure 5. The correspondence between color quality scale and $Mg_8Ge_2O_{11}F_2:Mn^{4+}$ concentration in 5600 K WLEDs

In which, Pλ is spectral power distribution (SPD) (mW/nm). h is Planck's constant (J.s). Speed of light is presented by c (m·s−1). λ is the wavelength in nm. Optical power of the light source is Popt (W). λpeak is peak wavelength where light reach the highest intensity (nm). Δλ Full-width at half-maximum (FWHM) (nm). The ratios of blue-green-yellow (B-G-Y) spectra to white spectrum, which are dimensionless, are expressed respectively as η_b, $\eta_g$and η_y.P_{opt_b}, P_{opt_g}, P_{opt_y} and P_{opt_total} is the optical power (W) of each individual spectrum of blue, green, yellow and white. λ_{peak_b}, λ_{peak_g} and λ_{peak_y} represent the peak wavelengths (nm) of the blue, green, yellow spectra while λ1, λ2 Wavelengths at half of the peak intensity.

$$P_\lambda = P_{opt\_b}\frac{1}{\sigma_b\sqrt{2\pi}}exp\left[-0.5*\frac{(\lambda-\lambda_{peak\_b})^2}{{\sigma_b}^2}\right] + P_{opt\_g}\frac{1}{\sigma_g\sqrt{2\pi}}exp\left[-0.5*\frac{(\lambda-\lambda_{peak\_g})^2}{{\sigma_g}^2}\right] + P_{opt\_y}\frac{1}{\sigma_y\sqrt{2\pi}}exp\left[-0.5*\frac{(\lambda-\lambda_{peak\_y})^2}{{\sigma_y}^2}\right] \quad (3)$$

$$P_\lambda = \eta_b P_{opt\_total}\frac{1}{\sigma_b\sqrt{2\pi}}exp\left[-0.5*\frac{(\lambda-\lambda_{peak\_b})^2}{{\sigma_b}^2}\right] + \eta_g P_{opt\_total}\frac{1}{\sigma_g\sqrt{2\pi}}exp\left[-0.5*\frac{(\lambda-\lambda_{peak\_g})^2}{{\sigma_g}^2}\right] + \eta_y P_{opt\_total}\frac{1}{\sigma_y\sqrt{2\pi}}exp\left[-0.5*\frac{(\lambda-\lambda_{peak\_y})^2}{{\sigma_y}^2}\right] \quad (4)$$

σ_b, σ_g and σ_y in turn are the FWHM-related coefficients (nm) for the blue, green, and yellow spectra. This mathematical models for SPC in WLEDs with phosphor layer can be perceived as a tricolor spectrum and an extended Gaussian model. The scattering of $Mg_8Ge_2O_{11}F_2:Mn^{4+}$ phosphor particle was analyzed by using the Mie-theory. In addition, the scattering cross section Csca for spherical particles can be computed by the following expression through applying the Mie theory. The calculation of total emitted light can base on Lambert-Beer law:

$$I = I0\ exp(-\mu extL) \quad (5)$$

The incident light power is expressed as I_0 in this formula. L represents the thickness of phosphor layer measured in mm. The extinction coefficient is μ_{ext} and can be determined through the equation of $\mu_{ext} = N_r.C_{ext}$, with N_r being the number density distribution of particles (mm^{-3}) and extinction cross-section of phosphor molecule is C_{ext} (mm^2).

The result of luminous flux analysis in dual-layer remote phosphor structure computed according to (5) shows superiority in comparison to the luminous flux of single-layer structure. It can be concluded that the advantage dual-layer remote phosphor structure has on the lighting properties enhancement comes from the addition of $Mg_8Ge_2O_{11}F_2:Mn^{4+}$, therefore, managing the concentration of $Mg_8Ge_2O_{11}F_2:Mn^{4+}$ is an

essential task. Even though the concentration of $Mg_8Ge_2O_{11}F_2:Mn^{4+}$ and the extinction coefficient μ_{ext} increase together according to the Lambert-Beer law, which improves the light absorption, the increase in $Mg_8Ge_2O_{11}F_2:Mn^{4+}$ concentration is unfavorable for the light energy transmission. In particular, the luminous flux declines if the alteration of phosphor layer thickness increase the concentration of $Mg_8Ge_2O_{11}F_2:Mn^{4+}$. The reduced luminous flux at all CCTs rises when $Mg_8Ge_2O_{11}F_2:Mn^{4+}$ concentration increase, and especially noticeable at 16% $Mg_8Ge_2O_{11}F_2:Mn^{4+}$. Concentration and the graph exhibited in Figure 6 is the practical example of the previous statement. Although the luminous flux is reduced when there is a presence of $Mg_8Ge_2O_{11}F_2:Mn^{4+}$, using red phosphor $Mg_8Ge_2O_{11}F_2:Mn^{4+}$ in dual-layer phosphor structure is still a suitable choice with the better overall performance considering the improvements it brings in the same concentration range to CRI from 68 rises to 78, CQS from 65 rises to 71, and the higher luminous flux compares to the single-layer structure. Therefore, the slight reduction in luminous is still reasonable as long as the overall performance is better. By considering the gain in CRI, CQS and loss in luminous flux with the results in this manuscript, the manufacturers can now choose an optimal percentage of $Mg_8Ge_2O_{11}F_2:Mn^{4+}$ concentration for the production of WLEDs in each unique case according to the predetermined properties.

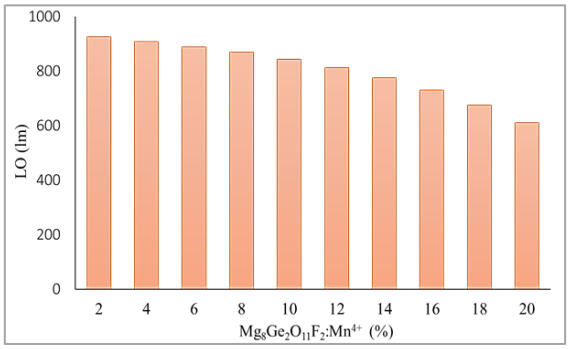

Figure 6. The luminous output (LO) responses to the presence of $Mg_8Ge_2O_{11}F_2:Mn^{4+}$ concentration in 5600 K WLEDs

4. CONCLUSION

Through numerous experiments that involves constant adjustments of the phosphor emission spectrum, this research has verified the effectiveness of $Mg_8Ge_2O_{11}F_2:Mn^{4+}$ and therefore, suggests it to be used dual-layer phosphor $Mg_8Ge_2O_{11}F_2:Mn^{4+}$ structure for lighting developments. Specifically, WLEDs with $Mg_8Ge_2O_{11}F_2:Mn^{4+}$ phosphor in their phosphor layer will have high CRI and CQS as well as the ability to adjust the color of white light. The only problem is the deteriorating luminous output in WLED package when $Mg_8Ge_2O_{11}F_2:Mn^{4+}$ concentration increase, therefore, manufacturers must consider a suitable phosphor concentration for this tradeoff between CRI, CQS and luminous flux. Although the application of $Mg_8Ge_2O_{11}F_2:Mn^{4+}$ may results in a decline in luminous flux, the light output value in dual-layer phosphor package is still acceptable because it is far more superior to that of the single-layer phosphor package. To serve the purpose of fabricating WLEDs with different shades of white lights, a quality enhancement structure was created from the theoretical application of Beer's law and linear conversion. According to the calculation from WLED at 5600 K CCT, the largest possible discrepancy between models is around 0.0063, which show that the measured and simulated CIE 1931 are not too dissimilar to cause diversion to the results, thus, ensure the reliability of the calculation conducted in this manuscript. This research shows positive results regarding the effectiveness of the new lighting configuration in improving the lighting performance.

ACKNOWLEDGEMENTS

This research is funded by Foundation for Science and Technology Development of Ton Duc Thang University (FOSTECT), website: http://fostect.tdtu.edu.vn, under Grant FOSTECT.2017.BR.06.

REFERENCES

[1] Z. Zhuang *et al.*, "Optimal ITO transparent conductive layers for InGaN-based amber/red light-emitting diodes," *Opt. Express,* vol. 28, no. 8, pp. 12311-12321, 2020.
[2] N. Q. Li *et al.*, "High-efficiency solution-processed WOLEDs with very high color rendering index based on a macrospirocyclic oligomer matrix host," *Optical Materials Express,* vol. 8, no. 10, pp. 3208-3219, 2018.

[3] J. Jia *et al.*, "Three-wavelength passive demodulation technique for the interrogation of EFPI sensors with arbitrary cavity length," *Opt. Express,* vol. 27, no. 6, pp. 8890-8899, 2019.
[4] N. D. Q. Anh, *et al.*, "Selection of a Remote Phosphor Configuration to Enhance the Color Quality of White LEDs," *Curr. Opt. Photon,* vol. 3, no. 1, pp. 78-85, 2019.
[5] X. Sun *et al.*, "Run-time reconfigurable adaptive LDPC coding for optical channels," *Opt. Express,* vol. 26, no. 2, pp. 29319-29329, 2018.
[6] H. Kim *et al.*, "Transparent effect on the gray scale perception of a transparent OLED display," *Opt. Express,* vol. 26, no. 4, pp. 4075-4084, 2018.
[7] C. Huang *et al.*, "Bandwidth correction of spectral measurement based on Levenberg-Marquardt algorithm with improved Tikhonov regularization," *Appl. Opt,* vol. 58, no. 9, pp. 2166-2173, 2019.
[8] S. Matsumoto *et al.*, "Chemical vapor deposition route to transparent thick films of Eu^{3+}-doped HfO_2 and Lu_2O_3 for luminescent phosphors," *Opt. Mater. Express,* vol. 10, no. 4, pp. 899-906, 2020.
[9] Y. Hu *et al.*, "Greatly enhanced persistent luminescence of $YPO_4:Sm^{3+}$ phosphors via Tb^{3+} incorporation for in vivo imaging," *Opt. Express,* vol. 28, no. 2, pp. 2649-2660, 2020.
[10] L. Qin *et al.*, "Luminance calculation method accounting for mesopic vision and fog penetration ability," *Appl. Opt,* vol. 59, no. 3, pp. 683-686, 2020.
[11] A. Ferrero *et al.*, "Index for the evaluation of the general photometric performance of photometers," *Opt. Express,* vol. 26, no. 14, pp. 18633-18643, 2018.
[12] A. K. Dubey *et al.*, "Laser-line-driven phosphor-converted extended white light source with uniform illumination," *Appl. Opt*, vol. 58, no. 9, pp. 2402-2407, 2019.
[13] N. T. Canh *et al.*, "Electrohydrodynamic jet-sprayed quantum dots for solution-processed light-emitting-diodes," *Opt. Mater. Express*, vol. 8, no. 12, pp. 3738-3747, 2018.
[14] B. Li *et al.*, "High-efficiency cubic-phased blue-emitting Ba3Lu2B6O15:Ce3+ phosphors for ultraviolet-excited white-light-emitting diodes," *Opt. Lett,* vol. 43, no. 20, pp. 5138-5141, 2018.
[15] J. Wang *et al.*, "Rapid 3D measurement technique for colorful objects employing RGB color light projection," *Appl. Opt*, vol. 59, no. 7, pp. 1907-1915, 2020.
[16] Y. Li *et al.*, "Bead-on-string fibers electrospun from terbium acetylacetonate hydrate doped poly methyl methacrylate," *Opt. Mater. Express,* vol. 8, no. 2, pp. 276-288, 2018.
[17] P. Zhu *et al.*, "Design rules for white light emitters with high light extraction efficiency," *Opt. Express,* vol. 27, no. 16, pp. A1297-A1307, 2019.
[18] Z. Liu *et al.*, "Effect of the replacement of Zn^{2+} with Mg^{2+} in $Ca_{14}Zn_6Ga_{10}O_{35}:Mn^{4+}$," *Opt. Mater. Express,* vol. 8, no. 9, pp. 2532-2541, 2018.
[19] N. Anous *et al.*, "Impact of blue filtering on effective modulation bandwidth and wide-angle operation in white LED-based VLC systems," *OSA Continuum,* vol. 1, no. 3, pp. 910-929, 2018.
[20] A. Kho *et al.*, "Compensating spatially dependent dispersion in visible light OCT," *Opt. Lett*, vol. 44, no. 4, pp. 775-778, 2019.
[21] R. Hirayama *et al.*, "Projection of multiple directional images on a volume structure with refractive surfaces," *Opt. Express*, vol. 27, no. 20, pp. 27637-27648, 2019.
[22] T. R. Dastidar *et al.*, "Whole slide imaging system using deep learning-based automated focusing," *Biomed. Opt. Express,* vol. 11, no. 1, pp. 480-491, 2020.
[23] F. Jiang *et al.*, "Efficient InGaN-based yellow-light-emitting diodes," *Photon. Res*, vol. 7, no. 2, pp. 144-148, 2019.
[24] Y. P. Chang *et al.*, "New scheme of LiDAR-embedded smart laser headlight for autonomous vehicles," *Opt. Express,* vol. 27, no. 20, pp. A1481-A1489, 2019.
[25] Y. J. Park *et al.*, "Development of high luminous efficacy red-emitting phosphor-in-glass for high-power LED lighting systems using our original low Tg and Ts glass," *Opt. Lett*, vol. 44, no. 24, pp. 6057-6060, 2019.
[26] X. Huang *et al.*, "High-efficiency and thermally stable far-red-emitting NaLaMgWO6:Mn4+ phosphorsfor indoor plant growth light-emitting diodes," *Opt. Lett*, vol. 43, no. 14, pp. 3305-3308, 2018.